BIOCHEMISTRY
including biophysical chemistry & molecular biology
Article

Biochemistry **2009,** *48,* 9525–9533 9525
DOI: 10.1021/bi9013209

Plasmodium falciparum Ferredoxin-NADP$^+$ Reductase His286 Plays a Dual Role in NADP(H) Binding and Catalysis‡

Danila Crobu,§ Giulia Canevari,§ Mario Milani,‖ Vittorio Pandini,§ Maria Antonietta Vanoni,§ Martino Bolognesi,§ Giuliana Zanetti,§ and Alessandro Aliverti*,§

§*Dipartimento di Scienze Biomolecolari e Biotecnologie, Università degli Studi di Milano, via Celoria 26, 20133 Milano, Italy, and* ‖*CNR-INFM-S3 c/o Dipartimento di Scienze Biomolecolari e Biotecnologie, Università degli Studi di Milano, via Celoria 26, 20133 Milano, Italy*

Received July 30, 2009; Revised Manuscript Received September 8, 2009

ABSTRACT: The NADP-binding site of *Plasmodium falciparum* ferredoxin-NADP$^+$ reductase contains two basic residues, His286 and Lys249, conserved within the *Plasmodium* genus, but not in other plant-type homologues. Previous crystal studies indicated that His286 interacts with the adenine ring and with the 5′-phosphate of 2′-P-AMP, a ligand that mimics the adenylate moiety of NADP(H). Here we show that replacement of His286 with aliphatic residues results both in a decrease in the affinity of the enzyme for NADPH and in a decrease in k_{cat}, due to a lowered hydride-transfer rate. Unexpectedly, the mutation to Gln produces an enzyme more active than the wild-type one, whereas the change to Lys destabilizes the nicotinamide−isoalloxazine interaction, decreasing k_{cat}. On the basis of the crystal structure of selected mutants complexed with 2′-P-AMP, we conclude that the His286 side chain plays a dual role in catalysis both by providing binding energy for NADPH and by favoring the catalytically competent orientation of its nicotinamide ring. For the latter function, the H-bonding potential rather than the positively charged state of the His286 imidazole seems sufficient. Furthermore, we show that the Lys249Ala mutation decreases K_m^{NADPH} and K_d for NADP$^+$ or 2′-P-AMP by a factor of 10. We propose that the Lys249 side chain participates in substrate recognition by interacting with the 2′-phosphate of NADP(H) and that this interaction was not observed in the crystal form of the enzyme−2′-P-AMP complex due to a conformational perturbation of the substrate-binding loop induced by dimerization.

Plasmodium falciparum and *Toxoplasma gondii*, as well as most apicomplexan parasites, possess a plastidic-type ferredoxin-NADP$^+$ reductase (FNR,[1] EC 1.18.1.2) (*1*−*5*), located in the apicoplast, a peculiar organelle evolutionarily related to plant plastids. As in nonphotosynthetic plant tissues, apicomplexan FNR transfers reducing equivalents from NADPH to ferredoxin (*2*) to fuel ferredoxin-dependent reductive apicoplast pathways. This function was experimentally shown for the mevalonate-independent production of isoprenoid precursors in *P. falciparum* (*6*). Some properties of *P. falciparum* FNR (PfFNR) are quite unusual among plastidic-type FNRs: a low turnover number, a peculiar NADP-binding site, and the ability to undergo a redox-dependent dimerization process that reversibly inactivates the enzyme (*4*, *7*).

We have previously described the NADP(H) binding by plastidic-type FNRs as a bipartite process, in which the 2′-P-AMP and the nicotinamide-ribose 5′-phosphate (NMN) moieties of the substrate interact with the enzyme in partially independent fashions (*8*). The 2′-P-AMP moiety plays a leading role in enzyme−substrate interaction: it remains bound to its subsite, while the NMN portion is essentially disordered, with the nicotinamide ring approaching the isoalloxazine moiety only for a fraction of time, sufficient to provide an adequate hydride-transfer (HT) rate (*9*). When this model is taken into account, the contacts that plastidic-type FNRs establish with NADP(H) during the catalytic cycle can be classified into two types: those that stabilize the FNR−NADP(H) complex, without affecting the conformation of the NMN moiety, and those that favor HT by orienting the nicotinamide ring toward the flavin. Protein residues interacting with the pyrophosphate group of NADP(H) are expected to play both roles, since, in addition to stabilizing the enzyme−substrate complex, they could affect the positioning of NMN. This is confirmed by the observation that Lys116 of spinach leaf FNR [corresponding to Arg100 of *Anabaena* FNR (*10*) and to Lys119 of PfFNR (*4*)] plays an essential role in catalysis by dramatically affecting k_{cat}/K_m^{NADPH} and significantly decreasing k_{cat} (*11*).

Whereas *T. gondii* FNR has a typical NADP-binding site, PfFNR displays a different distribution of basic groups in the region that binds the adenylate moiety of NADP(H). Plastidic-type FNRs primarily recognize NADP(H) through interactions with its 2′-phosphate group, which include two highly conserved hydrogen bonds provided by protein hydroxyls [Ser247 and Tyr258 in PfFNR (*4*)], and two salt bridges [involving Arg235 and Lys244 in spinach leaf FNR (*12*, *13*) and Arg224 and Arg233

‡Atomic coordinates and structure factors for PfFNR-H286L, PfFNR-H286L−2′-P-AMP, and PfFNR-H286K−2′-P-AMP species have been deposited in the Protein Data Bank as entries 3JQR, 3JQP, and 3JQQ, respectively.

*To whom correspondence should be addressed. Telephone: +39 02 50314897. Fax: +39 02 50314895. E-mail: alessandro.aliverti@unimi.it.

[1]Abbreviations: FNR, ferredoxin-NADP$^+$ reductase; PfFNR, *P. falciparum* FNR; NMN, nicotinamide-ribose 5′-phosphate; HT, hydride transfer; DCPIP, 2,6-dichlorophenolindophenol; CT, charge transfer; CT1, charge-transfer complex between NADPH and FAD; CT2, charge-transfer complex between NADP$^+$ and FADH$^-$; PDB, Protein Data Bank.

© 2009 American Chemical Society
Published on Web 09/08/2009

in *Anabaena* FNR (*14*)]. These basic residues are not conserved in PfFNR (*4*). On the other hand, in typical plastidic-type FNRs, the interaction with the NADP(H) adenosine involves an aliphatic side chain [Leu274 in spinach leaf FNR (*13*) and Leu263 in *Anabaena* FNR (*14*)], which belongs to a surface loop that has been proposed to contribute to pyridine nucleotide specificity (*12*, *14*−*16*). In PfFNR, this Leu residue is replaced with His286, which both engages a $\pi-\pi$ stacking interaction with the adenine and makes a contact with the 5′-phosphate of the substrate analogue 2′-P-AMP (*4*). This suggests that the function of His286 in catalysis could be more important than that played by the corresponding residue in other FNRs. To test this hypothesis, we have now generated and characterized a series of mutant enzymes in which His286 was changed to Gln, Lys, Ala, or Leu.

Another surprising feature of PfFNR is that no interaction between positively charged groups of the protein subunit and the 2′-phosphate of the ligand (*4*) was observed in the crystal structure of the dimeric enzyme in complex with 2′-P-AMP. However, conclusions about 2′-P-AMP binding by PfFNR should be drawn with caution from available crystallographic data since the NADP-binding site partially overlaps with the dimerization interface of the protein, implying that the conformation of this part of the macromolecule might be perturbed by intersubunit contacts. In particular, the side chain of Lys249, which in the crystal structure points away from the ligand, could adopt a different conformation in monomeric PfFNR in solution, playing a role in NADP(H) binding similar to that of Arg235 in spinach FNR. To test this hypothesis, we have produced and characterized a PfFNR mutant in which Lys249 was replaced with Ala.

The extensive characterization of the five PfFNR mutants reported here, which includes rapid kinetic studies and the determination of the crystal structures of two of them, allows us to conclude that, while both Lys249 and His286 play a role in NADP(H) binding, the interaction established by His286 with the pyrophosphate group of the substrate is critical for orienting the nicotinamide ring, thus favoring HT to FAD.

MATERIALS AND METHODS

Materials. $NADP^+$, NADPH, and 2′-P-AMP were purchased from Sigma-Aldrich. All other chemicals were of the highest commercially available grade.

Site-Directed Mutagenesis. The base changes required to make the amino acid replacements of His286 and Lys249 in PfFNR reported in this work were introduced into pET-PfFNR (*7*) using the QuikChange site-directed mutagenesis kit (Stratagene). The following couples of complementary oligonucleotides were used (base changes underlined): His286Gln, 5′-GAATTATATATATGTGGTCAGAAATCAATAAGATATAAAGTTATG-3′ and 5′-CATAACTTTATATCTTATTGATTCTGACCACATATATATAATTC-3′; His286Lys, 5′-GAATTATATATATGTGGTAAAAAATCAATAAGATATAAAGTTATG-3′ and 5′-CATAACTTTATATCTTATTGATTTTTTACCACATATATATAATTC-3′; His286Ala, 5′-GAATTATATATATGTGGTGCCAAATCAATAAGATATAAAGTTATG-3′ and 5′-CATAACTTTATATCTTATTGATTTGGCACCACATATATATAATTC-3′; His286Leu, 5′-GAATTATATATATGTGGTCTGAAATCAATAAGATATAAAGTTATG-3′ and 5′-CATAACTTTATATCTTATTGATTTCAGACCACATATATATAATTC-3′; Lys249Ala, 5′-TATACATTATGTTTTCTCTTATGCACAAAATTCAGATGCAACAAG-3′ and 5′-CTTGTTGCATCTGAATTTTGTGCATAAGAGAAAACATAATGTATA-3′. The plasmids carrying the mutations mentioned above were named pET-PfFNR-H286Q, pET-PfFNR-H286K, pET-PfFNR-H286A, pET-PfFNR-H286L, and pET-PfFNR-K249A, respectively. Each insert was fully sequenced to verify the presence of the desired base changes and rule out unwanted mutations.

Protein Overproduction and Purification. *Escherichia coli* Rosetta(DE3) cells, transformed with each one of the plasmids mentioned above, were grown as reported elsewhere (*7*). Wild-type and mutant PfFNR forms were purified according to the same procedure (*7*), which included metal chelate chromatography on Ni Sepharose (GE Healthcare) and hydrophobic interaction chromatography on Phenyl Sepharose (GE Healthcare). After treatment with factor Xa (Pierce) to cleave the N-terminal extension containing the poly-His tag, the mature PfFNR forms were isolated from the protease and residual uncleaved proteins by a second run on the Ni Sepharose column, to which they weakly bound because of the intrinsic affinity of PfFNR for Ni^{2+} (*4*).

Spectral Analyses. All absorption spectra were recorded on an 8453 diode-array (Agilent) or double-beam Cary 100 (Varian) spectrophotometer. The extinction coefficients of the mutant PfFNRs in the visible region of the spectrum were determined by measuring the amount of FAD released by each protein following sodium dodecyl sulfate treatment (*17*). Spectrophotometric active-site titrations with $NADP^+$ were conducted at 15 °C in 50 mM Tris-HCl (pH 7.6) as described previously (*4*). Anaerobic stepwise photoreduction of the FAD prosthetic group of PfFNR forms was performed by the light/EDTA system (*18*) at 15 °C. The enzymes were diluted to ~15 μM in 50 mM HEPES-NaOH (pH 7.0) containing 10% glycerol, 13 mM EDTA, and 1.3 μM 5-carba-5-deazariboflavin. $NADP^+$ was at a 1.2 molar ratio with respect to the enzyme. The solution was made anaerobic by successive cycles of equilibration with O_2-free nitrogen and evacuation.

Steady-State Kinetics. Both NADPH-dependent $K_3Fe(CN)_6$ and 2,6-dichlorophenolindophenol (DCPIP) activity assays were performed at 25 °C in 100 mM Tris-HCl (pH 8.2) in the presence of a NADPH-regenerating system formed by glucose 6-phosphate and glucose-6-phosphate dehydrogenase. The NADH-$K_3Fe(CN)_6$ reductase activity of the PfFNR-K249A form was measured as described above, but the NADPH-regenerating system was omitted. To estimate the steady-state kinetic parameters of the enzyme forms, the concentrations of NAD(P)H and the electron acceptor were independently varied. The inhibitory effect of 2′-P-AMP on the NADPH−DCPIP reductase reaction catalyzed by the PfFNR forms was studied by independently varying the concentration of NADPH and that of the inhibitor at a fixed concentration of DCPIP (20 μM).

Rapid Kinetics. Wild-type or mutant PfFNRs (17−20 μM) were reacted with NADPH (0.025−2 mM) at 25 °C in 50 mM HEPES-NaOH (pH 7.0) under anaerobic conditions, using an SF-61 DX2 diode-array stopped-flow spectrophotometer (Hi-Tech Scientific, Bradford-upon-Avon, U.K.). A set of 300 spectra within the 300−700 nm wavelength range was recorded from each shot over total reaction times ranging from 0.5 to 7 s. Absorbance traces at different wavelengths were fitted to exponential decay equations using KinetAsyst version 3.0 (Hi-Tech Scientific).

Crystallization and X-ray Diffraction Data Collection. Both PfFNR-H286L and PfFNR-H286K were crystallized in

Table 1: Data Collection and Refinement Statistics for the PfFNR Mutants

	PfFNR-H286L	PfFNR-H286L−2′-P-AMP	PfFNR-H286K−2′-P-AMP
	Data Collection		
resolution (Å)	40.0−2.3	61.3−3.0	83.9−2.2
space group	$C2$	$P3_1$	$P3_1$
mosaicity (deg)	0.8	0.8	0.8
R_{merge} (%)	14.5 (71.0)[a]	15.7 (77.5)[a]	11.4 (56.4)[a]
total no. of observations	79430 (11721)	175963 (24091)	361295 (53358)
no. of unique observations	14346 (2072)	44994 (6554)	111739 (17208)
mean I (standard deviation)	10.9 (2.2)	9.5 (1.7)	9.9 (1.8)
completeness (%)	99.9 (99.9)	100 (99.9)	100 (100)
multiplicity	5.5 (5.7)	3.9 (3.7)	3.1 (3.1)
	Refinement		
R/R_{free} (%)	22.7/29.0	24.41/31.66	25.6/30.8
root-mean-square deviation for bond lengths (Å)	0.005	0.012	0.006
root-mean-square deviation for angles (deg)	0.88	1.33	1.01
Ramachandran plot			
residues in most favored region (%)	90.4	85.5	89.3
residues in additional allowed region (%)	9.6	14.5	10.7

[a]Outer shell limits: 2.42−2.30 Å for PfFNR-H286L, 3.16−3 Å for PfFNR-H286L−2′-P-AMP, and 2.32−2.2 Å for PfFNR-H286K−2′-P-AMP.

batch setup under a 1:1 mixture of paraffin and silicon oils, using an Oryx 8 robot (Douglas Instruments Ltd.). We cocrystallized PfFNR-H286K with the substrate analogue 2′-P-AMP by mixing a 0.2 μL drop of protein solution (25 mg/mL PfFNR-H286K, containing 2 mM 2′-P-AMP and 1 mM DTT) with a 0.1 μL drop of precipitant [20% 2-propanol, 20% PEG 4000, and 0.1 M citrate-NaOH (pH 5.4)]. The 400 μm × 100 μm × 50 μm crystal used for data collection grew at 293 K in ∼2 weeks. PfFNR-H286L was crystallized both in its free form and in a complex with 2′-P-AMP. We obtained the PfFNR-H286L crystals by mixing a 0.2 μL drop of protein solution (35 mg/mL PfFNR-H286L, containing 1 mM DTT) with a 0.1 μL drop of precipitating solution [1.6 M citrate-NaOH (pH 6.5)], while we obtained the PfFNR-H286L−2′-P-AMP crystals by soaking a crystal [grown in 12% PEG 6000, 5% glycerol, and 0.1 M cacodylate-NaOH (pH 6.5)] in a stabilizing solution containing the ligand [18% PEG 6000, 5% glycerol, 0.1 M cacodylate-NaOH (pH 6.5), and 3 mM 2′-P-AMP]. The PfFNR-H286L and PfFNR-H286L−2′-P-AMP crystals grew at 293 K in ∼3 weeks, and their final dimensions were approximately 50 μm × 50 μm × 50 μm and 50 μm × 250 μm × 25 μm, respectively. All the crystals were soaked for ∼30 s in cryoprotectant solutions (obtained via addition of up to 25% glycerol to the respective precipitating solution) prior to being cryocooled in liquid nitrogen. X-ray diffraction data were collected at 100 K at ESRF, Grenoble, ID 23-1 (PfFNR-H286K−2′-P-AMP and PfFNR-H286L) and at Elettra, Trieste, XRD1 (PfFNR-H286L−2′-P-AMP). The data were indexed [MOSFLM (*19*)] and scaled [SCALA (*20*)], showing that, in the presence of 2′-P-AMP, the crystals of PfFNR-H286K and PfFNR-H286L belong to a primitive trigonal space group. The unit cell parameters are similar to those displayed by wild-type PfFNR−2′-P-AMP crystals (*4*), belonging to space group $P3_1$. As observed for the wild-type enzyme, the crystals of both PfFNR mutants complexed with 2′-P-AMP host six molecules in the asymmetric unit, arranged in three dimers, each dimer being stabilized by a disulfide bridge between Cys99 residues of adjacent molecules. The ligand-free PfFNR-H286L crystallized in monoclinic space group $C2$ with one molecule in the asymmetric unit and the following unit cell parameters: a = 82.1 Å, b = 96.7 Å, c = 46.8 Å, $\alpha = \gamma = 90°$, and $\beta = 118°$. Phasing was performed by molecular replacement using, as search models, the structure of the PfFNR−2′-P-AMP complex (PDB entry 2OK7) for the ligand-bound form of both enzyme mutants, and chain A of PfFNR (PDB entry 2OK8) for ligand-free PfFNR-H286L. The searches were conducted using MOLREP (*21*). The models were successively refined using REFMAC 5 (*22*) and optimized by manual rebuilding (*23*). Data collection and refinement statistics are reported in Table 1.

RESULTS

Overproduction and Purification of Mutant PfFNRs. Replacement of His286 with Gln, Lys, Ala, and Leu, as well as the Lys249Ala substitution, resulted in PfFNR mutants that were produced by *E. coli* in soluble form at levels very similar to that of the wild-type protein. They were purified to homogeneity with an overall yield comparable to that of wild-type PfFNR. These observations indicate that His286 and Lys249 have no relevant role in protein folding and stability. Notably, after removal of the His tag, all PfFNR mutants maintain the same ability to weakly bind to the metal chelate resin as the wild-type enzyme, ruling out a role for His286 or Lys249 in determining the affinity of PfFNR for Ni^{2+} (*6*). All mutant PfFNRs display extinction coefficients and spectral features indistinguishable from those of the wild-type enzyme, indicating that the engineered mutations do not perturb the conformation of the protein.

Catalytic Properties of the His286 Mutants of PfFNR. We have studied the NADPH-dependent diaphorase activities of four enzyme mutants carrying different replacements of His286. The effect of the mutations on the steady-state kinetic parameters for the NADPH−$K_3Fe(CN)_6$ reaction is highly dependent on the residue replacing His286 (Table 2). With the exception of the His286Gln replacement, which slightly increases k_{cat}, all the other mutations significantly decrease both k_{cat}/K_m^{NADPH} and k_{cat}. Since the interpretation of these data is complicated by the fact that the ferricyanide ion, besides being a substrate, behaves as a competitive inhibitor of PfFNR with respect to NADPH (*4*), we have also determined the kinetic parameters of most mutants

Table 2: Kinetic Parameters of PfFNR Forms in the NADPH-Dependent Diaphorase Reactions with Different Artificial Electron Acceptors

	NADPH−$K_3Fe(CN)_6$ reductase reaction				NADPH−DCPIP reductase reaction		
PfFNR	k_{cat} (e^- equiv s^{-1}) (%)	K_m^{NADPH} (μM)	k_{cat}/K_m^{NADPH} (e^- equiv s^{-1} μM^{-1}) (%)	$K_i^{Fe(CN)_6 3-}$ (μM)	k_{cat} (e^- equiv s^{-1}) (%)	K_m^{NADPH} (μM)	k_{cat}/K_m^{NADPH} (e^- equiv s^{-1} μM^{-1}) (%)
wild type	250 ± 8 (100)	36 ± 6	7.0 ± 1 (100)	230 ± 40	110 ± 3 (100)	71 ± 4	1.5 ± 0.1 (100)
H286Q	370 ± 6 (150)	57 ± 5	6.5 ± 0.6 (93)	110 ± 11	140 ± 11 (130)	22 ± 3	6.3 ± 0.9 (420)
H286K	7.6 ± 0.4 (3)	nd[a]	nd[a]	nd[a]	12.0 ± 0.7 (11)	140 ± 14	0.09 ± 0.01 (5.8)
H286A	89 ± 2 (36)	520 ± 55	0.17 ± 0.01 (2.4)	91 ± 11	35.0 ± 1.7 (32)	400 ± 40	0.098 ± 0.009 (6.5)
H286L	15 ± 0.6 (6)	370 ± 46	0.04 ± 0.005 (0.6)	91 ± 15	nd[b]	nd[b]	nd[b]

[a]Not determinable. A reliable estimate of K_m^{NADPH} was not possible because of the apparently very low value of $K_i^{Fe(CN)_6 3-}$ for the PfFNR-H286K mutant. [b]Not determinable. The kinetic parameters were not measured because of an anomalous reactivity of PfFNR-H286L with DCPIP.

Table 3: Parameters for the Inhibition by 2′-P-AMP of the PfFNR Forms in the NADPH−DCPIP Reductase Reaction and K_d Values of the Complexes between PfFNR and $NADP^+$[a]

PfFNR	$K_i^{2'\text{-P-AMP}}$ (μM)	$K_d^{NADP^+}$ (μM)
wild type	24 ± 2	60 ± 9
H286Q	71 ± 7	130 ± 10
H286K	2.9 ± 0.2	30 ± 5
H286A	230 ± 25	280 ± 90

[a]The $K_i^{2'\text{-P-AMP}}$ of PfFNR-H286L was not determined because of an anomalous reactivity of this enzyme mutant with DCPIP. Moreover, the very small spectral changes induced by binding of $NADP^+$ to PfFNR-H286L prevented a reliable estimate of the K_d value of the resulting complex.

using the electron acceptor DCPIP, which does not inhibit PfFNR. As shown in Table 2, the kinetic properties of the PfFNR forms measured with DCPIP are in good agreement with those observed using ferricyanide. In the NADPH−DCPIP reductase reaction, the His286Gln mutation, besides slightly increasing k_{cat}, strongly increases k_{cat}/K_m^{NADPH}. Again, all the other amino acid replacements negatively affect both k_{cat}/K_m^{NADPH} and k_{cat} (Table 2). Unexpectedly, steady-state kinetics indicated that the His286Leu mutation determines the largest decrease in k_{cat}/K_m^{NADPH}, while mutation to Lys yields the mutant with the lowest k_{cat} when ferricyanide is the electron acceptor (Table 2). This demonstrates that Leu, which is commonly found at this site in other plastidic-type FNRs, and Lys, carrying a positive charge suitable for interaction with the NADP(H) pyrophosphate, are not substitutes for His286 in PfFNR. To evaluate the role of the His286 side chain in binding the adenylate moiety of the substrate, we measured the inhibition constant displayed by 2′-P-AMP ($K_i^{2'\text{-P-AMP}}$), which acts as an inhibitor of the PfFNR forms, competitive with NADPH, in the DCPIP reductase reaction. $K_i^{2'\text{-P-AMP}}$ values can be taken as a rough estimate of the dissociation constant of the complexes between the PfFNR forms and the inhibitor. As shown in Table 3, the values of $K_i^{2'\text{-P-AMP}}$ of the mutant PfFNRs compare well with those of K_m^{NADPH} in the diaphorase reactions (Table 2). PfFNR-H286A shows the lowest affinity for the ligand, while PfFNR-H286Q is the mutant most similar to the wild-type protein. Interestingly, PfFNR-H286K displays an affinity for 2′-P-AMP 8-fold higher than that of wild-type PfFNR.

$NADP^+$ Binding to His286 Mutants of PfFNR. To further investigate the role of His286 in the stabilization of the enzyme−substrate complex, we studied the interaction of the PfFNR forms with $NADP^+$ by differential spectrophotometry. It is known that $NADP^+$ binding to plastidic-type FNRs perturbs the visible absorption spectrum of the protein-bound FAD (*8*).

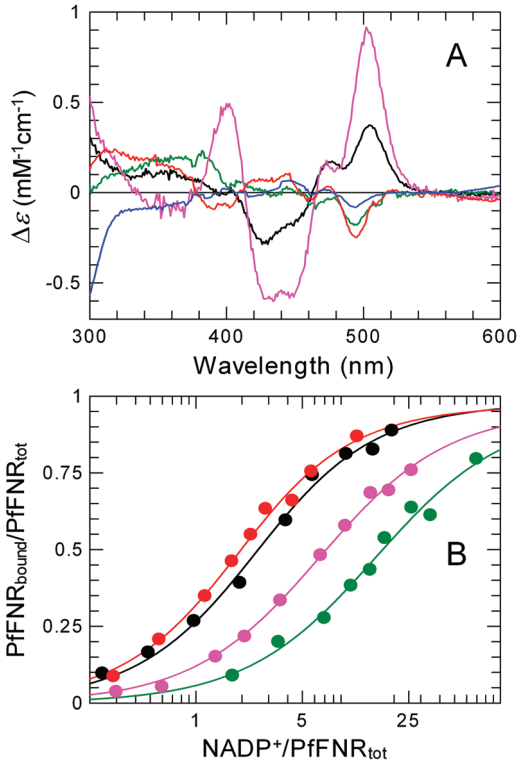

FIGURE 1: Interaction with $NADP^+$ of the His286 mutants of PfFNR. (A) Difference spectra of the enzyme−$NADP^+$ complexes. Difference spectra of the complexes of PfFNR (black), PfFNR-H286Q (magenta), PfFNR-H286K (red), and PfFNR-H286A (green) were computed by extrapolation to an infinite $NADP^+$ concentration. The difference spectrum of the PfFNR-H286L−$NADP^+$ complex (blue) was determined at 2 mM $NADP^+$, where no further spectral change was observed with an increase in the ligand concentration. (B) Spectrophotometric titration of PfFNR, PfFNR-H286Q, PfFNR-H286K, and PfFNR-H286A with $NADP^+$ at 15 °C in 50 mM Tris-HCl (pH 7.6) plotted using the same colors as in panel A. The fraction of bound enzyme was calculated from the spectral change observed after each $NADP^+$ addition. Each curve is the best fit of the data with the theoretical equation for 1:1 binding. Note the logarithmic scale of the horizontal axis.

Furthermore, it has been shown that the positive peak around 500 nm in the difference spectrum (Figure 1A) is due to the stacking interaction between the nicotinamide of $NADP^+$ and the FAD isoalloxazine ring (*24*). Thus, this experiment provides information about both the K_d for $NADP^+$ and the position of its nicotinamide ring within the complex. Figure 1B shows the titration curves of the PfFNR forms with $NADP^+$. In Table 3, the K_d values of the $NADP^+$ complexes are compared with the K_i values of 2′-P-AMP, showing similar trends. The difference

spectra of the mutant PfFNRs obtained at a saturating concentration of $NADP^+$ are markedly different from that of the wild-type enzyme (Figure 1A). In PfFNR-H286Q, the positive peak centered at 504 nm is much more intense than that observed with PfFNR. On the other hand, the spectra of the $NADP^+$ complex with either PfFNR-H286A or PfFNR-H286K display negative peaks at this wavelength. In terms of the bipartite binding mode of NADP(H) proposed for plant-type FNRs (*8*), the latter results indicate that, under $NADP^+$ saturating conditions, in PfFNR-H286Q the HT-competent position of the nicotinamide moiety of $NADP^+$ near the flavin *re* face is more populated than in PfFNR. On the other hand, the active site would be very poorly occupied by the nicotinamide moiety in the $NADP^+$ complex of the Ala, Leu, and Lys mutants. This conclusion provides a rationale for the effect of the mutations on the k_{cat} of the enzyme. Indeed, since $NADP^+$ and NADPH are expected to behave similarly as PfFNR ligands, the degree of access to the flavin by the nicotinamide ring of $NADP^+$ in the PfFNR forms is expected to correlate with the HT rate and, thus, with k_{cat}.

Charge-Transfer Complex Stabilization in PfFNR-H286Q and PfFNR-H286K. During redox titrations of FNRs, nicotinamide−flavin stacking interactions can be easily detected by the appearance of absorption bands above 600 nm, which are due to the formation of charge-transfer complexes between NADPH and FAD (CT1) and between $NADP^+$ and $FADH^-$ (CT2) (*24*, *25*). Thus, to verify that the change of His286 to Ala, Leu, or Lys hampers the HT-competent position of the nicotinamide, while the His286Gln mutation does not, we performed stepwise anaerobic photoreductions of PfFNR-H286Q and PfFNR-H286K in the presence of $NADP^+$ (Figure 2). As in the case of wild-type PfFNR, the peak at 454 nm of bound FAD becomes almost completely bleached in mutant PfFNRs before NADPH starts to accumulate, as evaluated by the increase in the absorbance at 340 nm. This observation suggests that the His286 mutations do not significantly affect the E_m of the flavin prosthetic group of PfFNR [previously measured to be -280 ± 2 mV at pH 7 (*7*)]. Interestingly, the amount of CT complex (most probably CT2), which in PfFNR was clearly observed in the late stages of the photoreduction (Figure 2A), was slightly but significantly higher in the case of PfFNR-H286Q (Figure 2B). Conversely, CT absorption bands were not detected in PfFNR-H286K (Figure 2C). These results, obtained under conditions similar to those of the rapid reaction studies (see below), confirm that the His286Gln mutation stabilizes the interaction between the redox-active moieties of bound NADP(H) and FAD, which is, instead, impaired by the His286Lys mutation.

Stopped-Flow Study of the Reaction of PfFNR-H286Q and PfFNR-H286L with NADPH. To evaluate the extent to which the His286 replacements affected HT from NADPH to FAD, two selected mutants, i.e., PfFNR-H286Q and PfFNR-H286L, were reacted with NADPH in a stopped-flow spectrophotometer. The composition of the reaction medium [50 mM HEPES-NaOH (pH 7.0)] was chosen to allow direct comparison with the data recently obtained for wild-type PfFNR (*7*) as well as other plastidic-type FNRs. Rapid reaction conditions are thus different from those under which the steady-state parameters were determined. The reaction of PfFNR with NADPH was previously described as a single-phase process, the rate constant of which is essentially independent of NADPH concentration (*7*). Here we performed a more extensive analysis of absorbance traces, which was extended to reaction times of >100 ms,

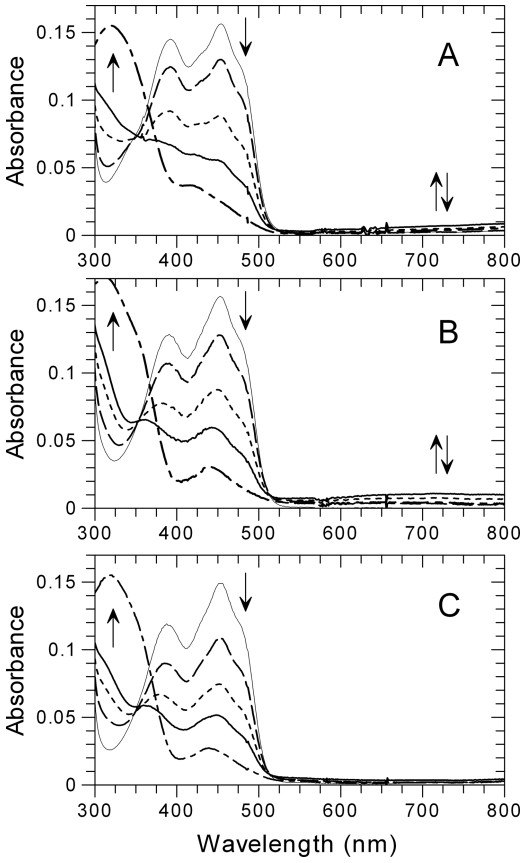

FIGURE 2: Anaerobic photoreduction of selected His286 mutants of PfFNR in the presence of $NADP^+$. Spectra of anaerobic mixtures of ~15 μM PfFNR (A), PfFNR-H286Q (B), and PfFNR-H268K (C) with 18 μM $NADP^+$ in 50 mM HEPES-NaOH (pH 7.0) containing 10% glycerol, recorded before (thin solid line) and after increasing irradiation times (1, 3, 5, and 12 min) with visible light. Arrows indicate the direction of the spectral changes.

allowing for observation of two phases. A first phase occurs with a k_{obs1} of ~150 s^{-1}, in which most of the absorption at 454 nm was lost. The second phase is much slower ($k_{obs2} = 8\ s^{-1}$) and accounts for ~10% of the total A_{454} change (Figures 3A and 4A,B). As previously reported, the reaction of the wild-type enzyme with NADPH involves the formation of a CT complex between NADPH and protein-bound FAD (CT1), which takes place within the dead time of the instrument (2 ms), followed by FAD reduction that can be observed as bleaching of the flavin absorbance bands (*7*). The fast observable phase was shown to correspond to the HT step of the catalytic cycle. The slow phase occurs at a rate that is too low to be compatible with catalysis and possibly represents a rearrangement of the reaction product (see below). As expected on the basis of its higher k_{cat} values, PfFNR-H286Q was found to react with NADPH considerably faster than the wild-type enzyme (Figures 3B and 4A,B). While the amplitude and the rate constant of the slow phase are essentially unchanged with respect to those of the wild-type enzyme, the k_{obs1} was found to be 240 s^{-1}, a value 1.7-fold higher than that of PfFNR (Figure 4C). It should be noted that, although more than half of the first phase occurred in the dead time, the first recorded spectrum shows a broad absorbance band extending above 550 nm, which can be attributed to CT complexes, which is slightly more intense than that recorded in the case of the wild-type enzyme (Figure 3A,B). Moreover, backward extrapolation of the absorbance to zero reaction time leads to an absorbance at

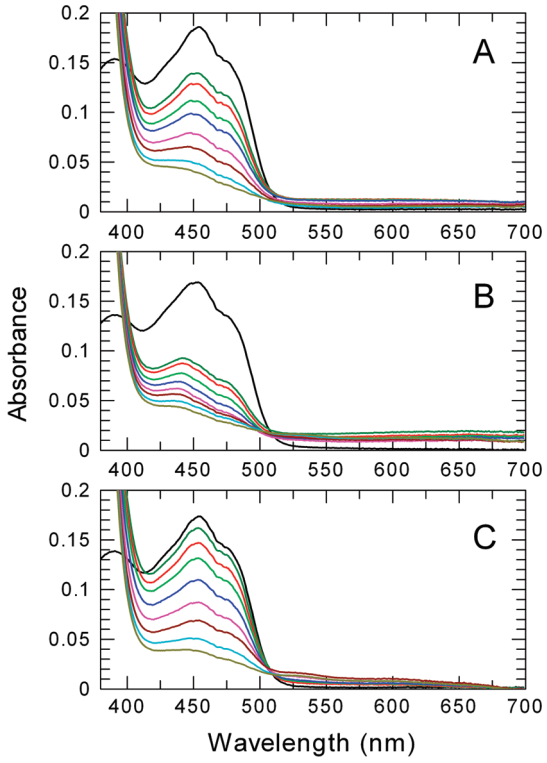

FIGURE 3: Spectra recorded during the reaction of selected His286 mutants of PfFNR with NADPH by stopped-flow spectrophotometry. PfFNR forms (17−18 μM) were reacted at 25 °C under anaerobiosis in 50 mM HEPES-NaOH (pH 7.0) with 500 μM NADPH (after mixing). (A) Spectra of oxidized PfFNR (black) and those recorded 1 ms (dark green), 2 ms (red), 5 ms (light green), 7 ms (blue), 11 ms (magenta), 17 ms (brown), 61 ms (aqua), and 1 s (olive) after mixing. (B) Spectra of oxidized PfFNR-H286Q (black) and those recorded 0.7 (dark green), 2.2 (red), 3.7 (light green), 6.7 (blue), 11 (magenta), 32 (brown), 110 (aqua), and 450 ms (olive) after mixing. (C) Spectra of oxidized PfFNR-H286L (black) and those recorded 2.2 ms (dark green), 6.7 ms (red), 14 ms (light green), 29 ms (blue), 76 ms (magenta), 320 ms (brown), 1 s (aqua), and 2.9 s (olive) after mixing.

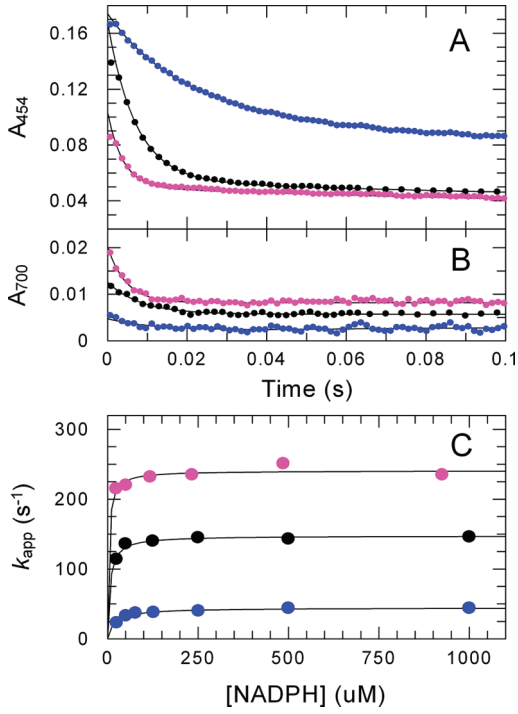

FIGURE 4: Absorbance traces and NADPH concentration dependence of the reductive half-reaction of selected His286 mutants of PfFNR, as studied by stopped-flow spectrophotometry. The PfFNR forms were reacted with NADPH at concentrations ranging from 25 μM to 1 mM (after mixing) as reported in the legend of Figure 3. (A) Absorbance at 454 nm recorded during the reaction of PfFNR (black), PfFNR-H286Q (magenta), and PfFNR-H286L (blue) with 500 μM NADPH. (B) Absorbance at 700 nm of the same reactions displayed in panel A. (C) Plot of the value of the rate constant of the fast phase of the reaction as a function of NADPH concentration (after mixing). Data from the three enzyme forms are identified by the same colors as those used in panels A and B. Fitting curves are rectangular hyperbolae. Limiting k_{obs1} values are 148 ± 2, 240 ± 4, and 44 ± 0.9 s^{-1} for PfFNR, PfFNR-H286Q, and PfFNR-H286L, respectively.

454 nm very close to that of the oxidized protein in the case of the PfFNR, but to a lower value (by ~0.03 unit) in the case of PfFNR-H286Q. These observations suggest that the initial enzyme−NADPH complex has a higher CT character in the mutant than in the wild-type enzyme, which most probably represents the cause of the higher HT rate observed with the mutant PfFNR form. The reactivity of PfFNR-H286L toward NADPH differs from that of PfFNR in three main aspects. First, the fast phase of FAD bleaching occurs with a rate constant k_{obs1} of 44 s^{-1} at saturating NADPH concentrations, a value significantly lower than that measured with PfFNR (Figure 4C). Consistently with this low HT rate, very little absorbance change attributable to CT interactions can be observed in the reaction of this mutant with NADPH (Figure 3C). Second, the slower phase of the reaction of PfFNR-H286L, while occurring with a rate similar to that observed with the other PfFNR forms, corresponds to a much larger spectral change (Figures 3C and 4C), accounting for ~50% of the total absorbance change at 454 nm for NADPH concentrations of < 100 μM. The amplitude of the slow phase was found to decrease as the NADPH concentration increased, while that of the first phase was found to increase. To provide a rationale for this behavior, we propose that the equilibrium between CT1 and CT2 is altered in PfFNR-H286L with respect to the wild-type enzyme (possibly as a result of a slight change in its redox potential), leaving a significant fraction of bound FAD in the oxidized form at the end of the first observable phase. The spectral features of the species accumulating during the subsequent slow phase suggest the presence of the blue semiquinone form of the flavin (Figure 3C). Therefore, we hypothesize that in this part of the process a reaction takes place between oxidized and reduced enzyme forms to yield the semiquinone species of bound FAD. Finally, as shown in Figure 4C, the value of k_{obs1} for the reaction of PfFNR-H286L with NADPH displays a dependence on the reductant concentration that is more marked than that observed with the two other enzyme forms, consistent with the higher values of K_m^{NADPH} of this mutant.

Structural Characterization of PfFNR-H286K and PfFNR-H286L. The overall crystal structures of PfFNR-H286L, the PfFNR-H286L−2′-P-AMP complex, and the PfFNR-H286K−2′-P-AMP complex bear very close resemblance to their wild-type analogues (PDB entries 2OK8 and 2OK7, in the absence and presence of 2′-P-AMP, respectively), thoroughly described elsewhere (*4*). As a matter of fact, root-mean-square deviations (rmsds) between corresponding mutant and wild-type forms, calculated for the Cα atoms of residues 5−316, excluding disordered surface loop regions, are comparable with those exhibited by different PfFNR molecules belonging to the same asymmetric unit. PfFNR, like other plastidic-type

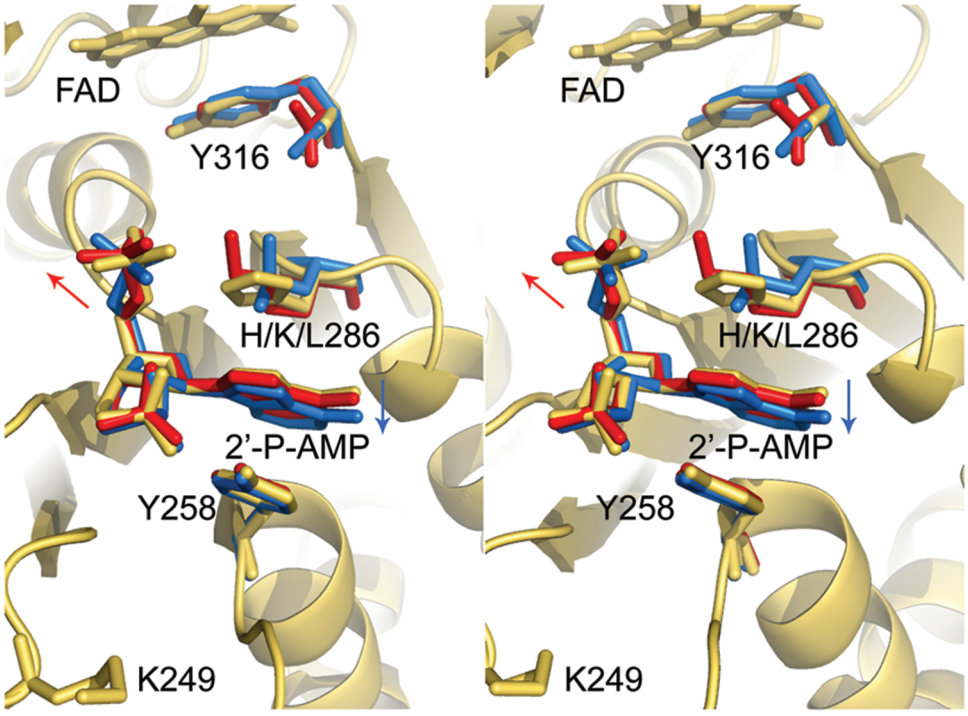

FIGURE 5: Binding of 2′-P-AMP to wild-type and mutant PfFNR forms. Stereoview of the crystal structures of the 2′-P-AMP complexes of PfFNR-H286K (red) and PfFNR-H286L (blue), superposed with that of wild-type PfFNR (yellow). The residues at position 286 and the 2′-P-AMP ligand are depicted as sticks in the context of the yellow cartoon of the wild-type protein. Also, part of the FAD prosthetic group, Lys249, Tyr258, and the C-terminal Tyr316 are shown. The two arrows indicate the direction of sliding of the adenine ring in the Leu mutant (blue) and displacement of 5′-phosphate in the Lys mutant (red). This figure was drawn using Pymol (DeLano Scientific, Palo Alto, CA).

FNRs, consists of an N-terminal FAD binding domain (residues 1−160) and a C-terminal $NADP^+$ binding domain (residues 166−316). The FAD domain hosts a β-barrel built of two perpendicular three-stranded antiparallel β-sheets ($\beta1\beta2\beta5$ and $\beta3\beta4\beta6$) and a single α-helix (αA), nestled between $\beta5$ and $\beta6$. The C-terminal domain consists of a five-stranded parallel β-sheet ($\beta9\beta8\beta7\beta10\beta11$), surrounded by seven α-helices (αB−αH). There are five disordered surface regions, corresponding to the N-terminus and the $\beta3-\beta4$, $\beta5-$αA, αB−$\beta9$, and αH−αI loops (residues 1−4, 63−97, 126−133, 96−205, and 299−305, respectively).

As previously mentioned (*4*), PfFNR undergoes a helix−coil transition upon 2′-P-AMP binding. In particular, helix αF is shortened by two turns at its N-terminus, while the $\beta9-$αF loop is correspondingly elongated by seven residues. The same behavior has been observed in PfFNR-H286L. Interestingly, in the case of PfFNR-H286L, ligand binding was obtained only after addition of a concentration of 2′-P-AMP 3-fold higher than that needed for the wild-type enzyme. This behavior is consistent with the decreased affinity of this mutant for the $NADP^+$ analogue (Table 3). On the other hand, in a manner consistent with its high affinity for the ligand (Table 3), PfFNR-H286K was easily crystallized in the presence of 2′-P-AMP.

Since the affinity of PfFNR for 2′-P-AMP is affected by the mutations of His286, we focused our attention on the 2′-P-AMP-binding site to explain the possible correlations between functional and structural aspects. In the PfFNR-H286L−2′-P-AMP crystal structure (3.0 Å resolution), the mutation affects mainly the binding mode of 2′-P-AMP, causing a displacement [Δ = 0.7 ± 0.1 Å (averaged over six molecules in the crystal asymmetric unit)] of its adenine end toward Tyr258, which in turn adjusts its position (Figure 5). The presence of the Leu286 residue, in fact, causes the loss of a stacking interaction between 2′-P-AMP and the protein, promoting a small sliding of the ligand toward the protein surface. In the case of PfFNR-H286K, a displacement (Δ = 0.5 ± 0.1 Å) of the 5′-phosphate occurs, likely due to the longer Lys side chain compared to His (Figure 5). Although small, this displacement can contribute to the destabilization of the nicotinamide−flavin interaction and thus be partly responsible for the low k_{cat} values of this mutant form (Table 2). Moreover, Lys286 can establish an electrostatic interaction with the carboxy terminus of Tyr316 (distance of 5.1 Å) that could restrict its mobility. Since displacement of the C-terminal Tyr is fundamental for the accessibility of the NADPH nicotinamide ring to the isoalloxazine moiety of FAD, this interaction might concur to hamper the catalytic activity of PfFNR-H286K.

Functional Properties of PfFNR-K249A. To evaluate the possible role of the the PfFNR Lys249 residue in NADPH recognition, we characterized the PfFNR-K249A mutant. While the k_{cat} values of this mutant in both NADPH-$K_3Fe(CN)_6$ and NADPH−DCPIP reductase reactions are not significantly affected (220 ± 5 and 110 ± 6 e^- equiv s^{-1}, respectively), the k_{cat}/K_m^{NADPH} ratio in the ferricyanide reductase reaction (0.73 ± 0.07 e^- equiv s^{-1} M^{-1}) was found to be 10-fold lower compared to that of the wild-type enzyme. On the other hand, the k_{cat}/K_m^{NADPH} ratio measured with DCPIP as the substrate is only slightly affected by the Lys249Ala mutation (1.0 ± 0.13 e^- equiv s^{-1} M^{-1}). To probe the affinity of the NADP(H)-binding site for its ligands, the interaction of PfFNR-K249A with 2′-P-AMP and $NADP^+$ was investigated by inhibition and titration studies, under the same conditions that were described for the His286 mutants. The K_i for 2′-P-AMP and the K_d for the $NADP^+$ complex were found to be 5.4- and 8.3-fold higher in the mutant than in the wild-type enzyme, respectively. The difference absorption spectrum of the PfFNR-K249A−$NADP^+$ complex was found to be very similar to that of the complex involving PfFNR.

Notably, the k_{cat}/K_m^{NADH} ratio of the mutant enzyme in the ferricyanide reductase reaction (0.13 ± 0.02 e^- equiv s^{-1} M^{-1}) is indistinguishable from that of the wild-type enzyme, ruling out the possibility that the Lys249 side chain interacts with groups other than the 2′-phosphate of the substrate nucleotide.

DISCUSSION

We have explored the possible role in catalysis of two basic residues located in the NADP(H)-binding site of PfFNR, i.e., Lys249 and His286. In a discussion of the steady-state kinetic properties of the mutant enzymes, it is useful to adopt the view originally proposed by Fersht (*26*), according to which the effect on catalysis of removal of a chemical group of the enzyme allows one to infer the step(s) of the catalytic cycle in which that group in the wild-type enzyme interacts with the substrate. The effect of a mutation on just the value of k_{cat}/K_m results from a uniform alteration of the binding energy of the enzyme for the substrate, both in the Michaelis complex and in the transition state of the chemical step of the catalyzed reaction, while the effect on k_{cat} results from the alteration of the binding energy for the substrate in the transition state only. Catalysis of HT in plant-type FNRs requires the conversion of the ground state of NADPH in the Michaelis complex, where the NMN portion of the substrate is disordered, to a transition state where the nicotinamide stacks onto the flavin ring according to a precise geometry. Since here we consider residues that are involved in NADP(H) binding but are located far from the site where HT occurs, their replacement cannot directly affect HT. Rather, they can influence the reductive half-reaction in two possible ways: (i) by altering the affinity for NADP(H) (thus affecting k_{cat}/K_m^{NADPH}) or (ii) by altering the orientation of the NMN moiety of bound NADP(H) (thus affecting k_{cat}).

Lys249 is located within the NADP(H) adenylate-binding loop of PfFNR. No interaction was detected between this residue and the ligand in the crystal structure of the dimeric form of the PfFNR−2′-P-AMP complex (*4*). However, we argued that Lys249 would be sufficiently flexible in solution to let its side chain reach the 2′-phosphate of the bound substrate. Indeed, the Lys249Ala replacement results in a 10-fold decrease in k_{cat}/K_m^{NADPH} with no effect on the k_{cat} of the ferricyanide reductase reaction. The role of Lys249 in substrate binding was confirmed by 2′-P-AMP inhibition and $NADP^+$ binding studies. The meaning of the mild effect of the mutation on the DCPIP reductase reaction is unclear, although it could be due to the fact that the rate of this reaction is limited by the enzyme oxidative half-reaction. Finally, the Lys249Ala mutation has no effect on the NADH-dependent activity of PfFNR, confirming that the group of NADP(H) interacting with the Lys249 side chain is indeed the 2′-phosphate. As a whole, these results indicate that the positively charged side chain of Lys249 provides a small contribution to the substrate binding energy (4−5.7 kJ/mol) and has no role in the stabilization of the HT-competent conformation of bound NADPH.

The replacement of PfFNR His286 resulted in more complex effects, which depend on the replacement residue. Deletion of the imidazole group by the His286Ala mutation markedly decreases k_{cat}/K_m^{NADPH} (by 15−40-fold, depending on the electron acceptor) and has a significant effect on k_{cat}, which is lowered to approximately one-third of that of the wild-type enzyme. Thus, His286 seems to have a critical role not only in NADP(H) binding but also in orienting the NMN moiety of the bound substrate to favor HT to FAD. This conclusion was confirmed by 2′-P-AMP inhibition and $NADP^+$ binding studies, where an affinity decrease by a factor of 5−10 was observed. Unexpectedly, replacement of His286 with Leu, which is present at this site in most plastidic-type FNRs, impaired the catalytic activity of PfFNR to an even greater extent than the mutation to Ala. The crystal structure of the PfFNR-H286L−2′-P-AMP complex showed that the mutation determines a significant shift in the position of the bound substrate analogue, which could explain the destabilization of the ordered HT-competent conformation of the NMN moiety of bound NADP(H). These conclusions are substantiated by the rapid kinetic studies, which showed that in this enzyme form the CT complexes are destabilized and HT proceeds at a rate 3.4-fold lower than in the wild-type enzyme. Such results underscore the notion that the imidazole ring of PfFNR His286 establishes with NADP(H) critical contacts for catalysis, which an aliphatic group cannot form. Surprisingly, PfFNR-H286K was the mutant with the lowest k_{cat}. Since this enzyme form binds 2′-P-AMP and $NADP^+$ with high affinity, we concluded that the His289Lys mutation specifically destabilized the HT-competent conformation that NADPH adopts in the transition state. The crystal structure of the complex of this protein mutant with 2′-P-AMP suggests that this effect can be due to either a slight displacement of the pyrophosphate group of bound NADP(H), which can be transmitted to the NMN moiety, or the salt bridge between the Lys289 ε-NH_3^+ group and the C-terminal carboxylate, which could compete with nicotinamide−isoalloxazine stacking. Finally, replacement of His286 with Gln resulted in an enzyme form that was highly active as a diaphorase and maintained ligand binding properties similar to those of the wild-type enzyme. PfFNR-H286Q displays a k_{cat} significantly higher than that of PfFNR, due to a 1.6-fold increase in the HT rate, as shown by stopped-flow studies. $NADP^+$ induced more intense spectral perturbations when bound to PfFNR-H286Q than to PfFNR, and greater amounts of CT species were observed in the case of this mutant form with respect to PfFNR during enzyme photoreduction in the presence of $NADP^+$ and as a transient during enzyme reaction with NADPH, as studied by rapid mixing. These observations indicate that the higher k_{cat} values of PfFNR-H286Q are due to a better stabilization provided by Gln, compared to His, of the HT-competent conformation of NADPH.

In summary, the two basic residues located in the adenylate-binding subsite of PfFNR, i.e., Lys249 and His286, both play a significant, although not essential, role in NADP(H) binding. The contributions provided by the two side chains to the binding energy of the HT-competent conformation of NADP(H) can be estimated to be ~5 and ~9 kJ/mol, respectively. However, while Lys249 contributes uniformly to binding of the ground- and transition-state conformations of the substrate by interacting with its 2′-phosphate, His286 also plays a role in favoring the HT-competent conformation of NADP(H), by interacting with its pyrophosphate group. Thus, as far as specific interactions with the adenylate moiety of NADP(H) are concerned, two major conclusions about PfFNR can be drawn. First, it is worth pointing out that protein engineering has allowed us to identify a cryptic enzyme−substrate interaction not detectable in crystal structures. The energetics of the ionic bond that the side chain of PfFNR Lys249 establishes with the 2′-phosphate of the substrate seems very similar to that formed by Arg224 of *Anabaena* FNR. Indeed, replacement of Arg224 of *Anabaena* FNR with Gln resulted in a 13-fold decrease in k_{cat}/K_m^{NADPH} without any effect

on k_{cat} (*27*). Thus, PfFNR Lys249 can be considered to be functionally equivalent to the conserved Arg located in the NADP-binding loop of other plastidic-type FNRs (Arg224 and Arg235 in *Anabaena* and spinach, respectively), although its location in sequence is shifted by one position. Second, PfFNR His286 plays an important role in catalysis, which is unprecedented in other plant-type FNRs. His286 of PfFNR is particularly important in favoring the HT-competent conformation of the bound substrate, a function that the corresponding Leu263 of *Anabaena* FNR does not play. Replacement of the corresponding Leu with Ala in *Anabaena* FNR was shown to have a minor effect on NADP(H) binding and essentially no consequence on HT (*15*). Here we propose that the interaction of His286 with the pyrophosphate group of NADP(H) is critical in orienting the NMN moiety of the substrate toward the flavin ring. The hydrogen bonding potential of the His286 side chain, rather than its possible ionic character, seems to be essential for this function, since the His286Gln mutation does not impair the catalytic properties of the enzyme, and even favors CT interactions and HT, while the His286Lys replacement dramatically slows turnover.

REFERENCES

1. Vollmer, M., Thomsen, N., Wiek, S., and Seeber, F. (2001) Apicomplexan parasites possess distinct nuclear-encoded, but apicoplast-localized, plant-type ferredoxin-NADP$^+$ reductase and ferredoxin. *J. Biol. Chem. 276*, 5483–5490.
2. Pandini, V., Caprini, G., Thomsen, N., Aliverti, A., Seeber, F., and Zanetti, G. (2002) Ferredoxin-NADP$^+$ reductase and ferredoxin of the protozoan parasite *Toxoplasma gondii* interact productively in vitro and in vivo. *J. Biol. Chem. 277*, 48463–48471.
3. Seeber, F., Aliverti, A., and Zanetti, G. (2005) The plant-type ferredoxin-NADP$^+$ reductase/ferredoxin redox system as a possible drug target against apicomplexan human parasites. *Curr. Pharm. Des. 11*, 3159–3172.
4. Milani, M., Balconi, E., Aliverti, A., Mastrangelo, E., Seeber, F., Bolognesi, M., and Zanetti, G. (2007) Ferredoxin-NADP$^+$ reductase from *Plasmodium falciparum* undergoes NADP$^+$-dependent dimerization and inactivation: Functional and crystallographic analysis. *J. Mol. Biol. 367*, 501–513.
5. Stelter, K., El-Sayed, N. M., and Seeber, F. (2007) The expression of a plant-type ferredoxin redox system provides molecular evidence for a plastid in the early dinoflagellate *Perkinsus marinus*. *Protist 158*, 119–130.
6. Rohrich, R. C., Englert, N., Troschke, K., Reichenberg, A., Hintz, M., Seeber, F., Balconi, E., Aliverti, A., Zanetti, G., Kohler, U., Pfeiffer, M., Beck, E., Jomaa, H., and Wiesner, J. (2005) Reconstitution of an apicoplast-localised electron transfer pathway involved in the isoprenoid biosynthesis of *Plasmodium falciparum*. *FEBS Lett. 579*, 6433–6438.
7. Balconi, E., Pennati, A., Crobu, D., Pandini, V., Cerutti, R., Zanetti, G., and Aliverti, A. (2009) The ferredoxin-NADP$^+$ reductase/ferredoxin electron transfer system of *Plasmodium falciparum*. *FEBS J. 276*, 3825–3836.
8. Deng, Z., Aliverti, A., Zanetti, G., Arakaki, A. K., Ottado, J., Orellano, E. G., Calcaterra, N. B., Ceccarelli, E. A., Carrillo, N., and Karplus, P. A. (1999) A productive NADP$^+$ binding mode of ferredoxin-NADP$^+$ reductase revealed by protein engineering and crystallographic studies. *Nat. Struct. Biol. 6*, 847–853.
9. Aliverti, A., Pandini, V., Pennati, A., de Rosa, M., and Zanetti, G. (2008) Structural and functional diversity of ferredoxin-NADP$^+$ reductases. *Arch. Biochem. Biophys. 474*, 283–291.
10. Martinez-Julvez, M., Hermoso, J., Hurley, J. K., Mayoral, T., Sanz-Aparicio, J., Tollin, G., Gomez-Moreno, C., and Medina, M. (1998) Role of Arg100 and Arg264 from *Anabaena* PCC 7119 ferredoxin-NADP$^+$ reductase for optimal NADP$^+$ binding and electron transfer. *Biochemistry 37*, 17680–17691.
11. Aliverti, A., Lubberstedt, T., Zanetti, G., Herrmann, R. G., and Curti, B. (1991) Probing the role of lysine 116 and lysine 244 in the spinach ferredoxin-NADP$^+$ reductase by site-directed mutagenesis. *J. Biol. Chem. 266*, 17760–17763.
12. Karplus, P. A., and Faber, H. R. (2004) Structural Aspects of Plant Ferredoxin: NADP$^+$ Oxidoreductases. *Photosynth. Res. 81*, 303–315.
13. Bruns, C. M., and Karplus, P. A. (1995) Refined crystal structure of spinach ferredoxin reductase at 1.7 Å resolution: Oxidized, reduced and 2′-phospho-5′-AMP bound states. *J. Mol. Biol. 247*, 125–145.
14. Serre, L., Vellieux, F. M., Medina, M., Gomez-Moreno, C., Fontecilla-Camps, J. C., and Frey, M. (1996) X-ray structure of the ferredoxin: NADP$^+$ reductase from the cyanobacterium *Anabaena* PCC 7119 at 1.8 Å resolution, and crystallographic studies of NADP$^+$ binding at 2.25 Å resolution. *J. Mol. Biol. 263*, 20–39.
15. Tejero, J., Martinez-Julvez, M., Mayoral, T., Luquita, A., Sanz-Aparicio, J., Hermoso, J. A., Hurley, J. K., Tollin, G., Gomez-Moreno, C., and Medina, M. (2003) Involvement of the pyrophosphate and the 2′-phosphate binding regions of ferredoxin-NADP$^+$ reductase in coenzyme specificity. *J. Biol. Chem. 278*, 49203–49214.
16. Karplus, P. A., Daniels, M. J., and Herriott, J. R. (1991) Atomic structure of ferredoxin-NADP$^+$ reductase: Prototype for a structurally novel flavoenzyme family. *Science 251*, 60–66.
17. Aliverti, A., Curti, B., and Vanoni, M. A. (1999) Identifying and quantitating FAD and FMN in simple and in iron-sulfur-containing flavoproteins. *Methods Mol. Biol. 131*, 9–23.
18. Massey, V., and Hemmerich, P. (1977) A photochemical procedure for reduction of oxidation-reduction proteins employing deazariboflavin as catalyst. *J. Biol. Chem. 252*, 5612–5614.
19. Leslie, A. G. W. (1999) Integration of macromolecular diffraction data. *Acta Crystallogr. D55*, 1696–1702.
20. Evans, P. R. (1993) Data reduction: Data correction and processing. In Proceedings of the CCP4 Study Weekend. Data Collection and Processing (Sawyer, L., Isaacs, N., and Bailey, S., Eds.) pp 114−123, Daresbury Laboratory, Warrington, U.K.
21. Vagin, A., and Teplyakov, A. (1997) MOLREP: An Automated Program for Molecular Replacement. *J. Appl. Crystallogr. 30*, 1022–1025.
22. Murshudov, G. N., Vagin, A. A., and Dodson, E. J. (1997) Refinement of Macromolecular Structures by the Maximum-Likelihood Method. *Acta Crystallogr. D53*, 240–255.
23. Emsley, P., and Cowtan, K. (2004) Coot: Model-building tools for molecular graphics. *Acta Crystallogr. D60*, 2126–2132.
24. Piubelli, L., Aliverti, A., Arakaki, A. K., Carrillo, N., Ceccarelli, E. A., Karplus, P. A., and Zanetti, G. (2000) Competition between C-terminal tyrosine and nicotinamide modulates pyridine nucleotide affinity and specificity in plant ferredoxin-NADP$^+$ reductase. *J. Biol. Chem. 275*, 10472–10476.
25. Aliverti, A., Deng, Z., Ravasi, D., Piubelli, L., Karplus, P. A., and Zanetti, G. (1998) Probing the function of the invariant glutamyl residue 312 in spinach ferredoxin-NADP$^+$ reductase. *J. Biol. Chem. 273*, 34008–34015.
26. Fersht, A. (1999) Structure and Mechanism in Protein Science: A Guide to Enzyme Catalysis and Protein Folding , W. H. Freeman & Co., New York.
27. Medina, M., Luquita, A., Tejero, J., Hermoso, J., Mayoral, T., Sanz-Aparicio, J., Grever, K., and Gomez-Moreno, C. (2001) Probing the determinants of coenzyme specificity in ferredoxin-NADP$^+$ reductase by site-directed mutagenesis. *J. Biol. Chem. 276*, 11902–11912.